Journal Pre-proofs

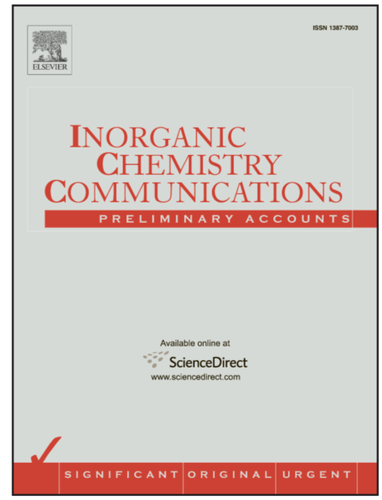

Short communication

Characterization of jet nebulizer spray pyrolysis coated MoS_2 thin films and fabrication of p-Si/n-MoS_2 junction diodes for optoelectronic application

T. Sasikala, K. Shanmugasundaram, P. Thirunavukkarasu, J. Chandrasekaran, P. Vivek, R. Marnadu, M. Aslam Manthrammel, S. Gunasekaran

PII: S1387-7003(21)00256-2
DOI: https://doi.org/10.1016/j.inoche.2021.108701
Reference: INOCHE 108701

To appear in: *Inorganic Chemistry Communications*

Received Date: 19 March 2021
Revised Date: 24 May 2021
Accepted Date: 29 May 2021

Please cite this article as: T. Sasikala, K. Shanmugasundaram, P. Thirunavukkarasu, J. Chandrasekaran, P. Vivek, R. Marnadu, M. Aslam Manthrammel, S. Gunasekaran, Characterization of jet nebulizer spray pyrolysis coated MoS_2 thin films and fabrication of p-Si/n-MoS_2 junction diodes for optoelectronic application, *Inorganic Chemistry Communications* (2021), doi: https://doi.org/10.1016/j.inoche.2021.108701

Characterization of jet nebulizer spray pyrolysis coated MoS_2 thin films and fabrication of p-Si/n-MoS_2 junction diodes for optoelectronic application

T. Sasikala[a], K. Shanmugasundaram[a,*,shanmugam.nks@gmail.com], P. Thirunavukkarasu[a], J. Chandrasekaran[b], P. Vivek[b], R. Marnadu[b], M. Aslam Manthrammel[c], S. Gunasekaran[d]

[a]Department of Electronics, Sri Ramakrishna Mission Vidyalaya College of Arts and Science, Coimbatore, 641 020, Tamil Nadu, India

[b]Department of Physics, Sri Ramakrishna Mission Vidyalaya College of Arts and Science, Coimbatore, 641 020, Tamil Nadu, India

[c]Department of Physics, Faculty of Science, King Khalid University, P.O. Box 9004, Abha, Saudi Arabia

[d]Department of Physics, PSG College of Arts and Science, Coimbatore-641014, Tamil Nadu, India

*Corresponding author.

Graphical abstract

Highlights

A nanostructured MoS_2 thin films were prepared on glass substrate by JNSP technique.

The elongated irregular rod-like structures were revealed through FESEM

The MoS_2 films deposited at 450°C exhibit minimum band gap.

We have fabricated p-Si/n-MoS_2 junction diode for different substrate temperature

A minimum ideality factor of 2.23 was obtained for 550 °C

Abstract

Inorganic two-dimensional materials are gradually becoming resources for modern electronic device manufacturing. Fascinate of 2D transition metal dicholgonides (TMDs) are particularly high. TMDS are very great potential for their characteristics and band gap structure in optoelectronic devices. In TMDs, 2D MoS_2 is most researchable material due to its good performance and its adequacy of electronic and optoelectronic application. Here we demonstrate MoS_2 thin film for various temperature such as 400, 450, 500, 550°C via Jet

Nebulizer Spray Pyrolysis (JNSP) technique for PN diode application. XRD pattern revealed that the polycrystalline nature of MoS_2 films with hexagonal crystal structure. The elongated irregular rod-like structures were revealed through FESEM. Elemental confirmation studies of Mo and S were done through EDX. The MoS_2 films deposited at 550°C exhibit minimum band gap. The average conductivity values were found to be increased from 1.730×10^{-8} to 3.877×10^{-7} S/cm with substrate temperature. A positive photo conducting-nature of p-Si/n-MoS_2 diode have been fabricated. Remarkably, the p-Si/n-MoS_2 diode fabricated at 550 ºC revealed minimum n values of 2.23.

Keywords: MoS_2 thin films; P-N junction diode; spray pyrolysis; I-V characterization

1. Introduction

Recently, two dimensional (2D) layered transition metal dichalcogenide (TMD) materials like disulphides and diselenides of Molybdenum (MoS_2 and $MoSe_2$) and Tungsten (WS_2 and WSe_2), Zirconium Disulfide (ZrS_2) and Rhenium disulphide (ReS_2) [1-6] are transpiring as exciting peer group materials for production of thin electronics devices. Among these TMD materials, a MoS2 thin film in particular has gained significant interest with research community due to its remarkable optical, electrical and optoelectronic properties. The bulk MoS_2 in general have reported an indirect transition nature with the energy gap of 1.2 eV and its direct energy gap is around 1.8eV [7]. It has carrier mobility 1-40 (cm^2/Vs) [8], higher optical absorption [9], high current switching ratio (~10^8) [10] and a strong excitonic binding energy [11] and fast photo-response [12]. In the last decade, various MoS_2 thin films were developed in order to improve their optoelectronic properties [13-17]. Sungjin Wi et al., [18] have fabricated plasma-assisted p-n junctions in multilayer MoS_2 photovoltaic (PV) devices which results good power, high photocurrent up to 20.9 mA/cm^2 and high external quantum efficiencies. Yuka Tsuboi et al., [19] demonstrated photovoltaic performances of solar cells were significantly archived higher PV efficiency of 11.1%. Meng-Lin Tsai et al., [20] reported the peak power conversion efficiency for PV cells based on monolayer TMD, where they observed 5.23% efficiency. Chung-Che Huang et al., [21] reported that nano-scale MoS_2 thin films were promising materials for optoelectronic applications. These authors found that the substrate material and annealing temperature plays a remarkable role in formation of single crystalline structure in MoS_2 thin films. In this context, C. Jiang et al., [22] developed transistors for high temperature application using MoS_2 thin films their operating temperature range upon 500K. Juhong Park et al.,[10] reported optical and electrical parameters form their studies the optical transparency more than 90%, electrical mobility of ~12.24 cm^2V^{-1} s^{-1} and $I_{on/off}$ ratio of ~10^6 obtained in prepared MoS_2 thin films and authors claimed these films flexible electronic applications compared with organic films. Yijin Zhang et al., [23] demonstrated that a thin transistor made of p-type MoS_2 achieved a high switching ratio for FET operations, and high hole mobility (μ_{max}~ 86 $cm^2\ V^{-1}\ s^{-1}$), which is double of electron mobility. Meanwhile, in the recent year's researchers have developed MoS_2 thin films for various application including photodetectors [24,25], gates [26], transistors [27], flexible biosensors [28] and light emitting diodes [29]. Until now, various methods have been adopted such us chemical vapour deposition [30], sputtering [31], atmospheric-pressure hydrogen reduction [32], chemical bath deposition method [33], sol-gel [34], solar cell [35], plasma evaporation [36] and spray pyrolysis. Ju Hyeong Kim et al., [37] have reported MoS_2 film by spray pyrolysis method. Until now, no articles have reported about preparation of Molybdenum disulphide (MoS_2) thin film using particular JNSP techniques. The JNSP technique has many advantage and is widely adopted in laboratories because of its simple handling method, low cost, better surface uniformity, extensive choice of precursors ability to control particle shape and size, composition and phase homogeneity of the film, capacity to produce large area high quality films of uniform thickness, the addition of dopants to the spray solution is simple, it is easy to prepare films of any composition by simply mixing the components in the appropriate ratios [38].

In this work, we have developed MoS_2 thin films with various substrate temperatures, 400, 450, 500 and 550 °C via JNSP techniques. Since it has several benefits like cost-effective, simple experimental setup, uniform coating, less operating temperature and small amount of precursor solution enough to get purity in films. Moreover, the prepared films were characterized by XRD, RAMAN, FESEM, UV-vis spectrometer and I-V characteristics for investigate the structural, optical and electrical properties of these MoS_2 thin films. Further, we have fabricated MoS_2 thin film based hetrojunction diodes. Here in there are many diode parameters were explored including saturation current (I_0), ideality factor (n), barrier height (Φ), for various substrate temperatures.

2 Experimental procedure

2.1 Materials

An Aqueous solution or uncongealed solution of Molybdenum Disulphide (MoS_2), (99.8%), glass substrates, 1×1cm p- silicon wafers, hydrochloric acid and isopropanol are procured from SIGMA Aldrich. The nebulizer kit was purchased from medical shop.

2.2. Preparation of MoS2 thin films

Nanostructured MoS_2 films were coated using various substrate temperature through JNSP technique using the RT mixed solution prepared by dissolving 0.05M of MoS_2 in HCL with continuous stirrer for 30 min. The spray pyrolysis has been employed on the thoroughly cleaned glass substrates (2 cm x 2.5 cm) at various substrate temperature; viz. 400, 450, 500 and 550 °C. The spray nozzle - substrate distance was kept at 5 cm. Pure MoS_2 Nano plate films were successfully grown as material droplets undergoing thermal decomposition at different substrate temperatures. The complete experimental setup of JNSP technique is shown in Fig. 1.

2.3 Assembly of p-Si/n-MoS_2 diodes

MoS_2 Nano plate /p-Si diodes are grown on 1 cm× 1 cm p-Si substrate. Initially, the undesired surface oxide layer and impurities were removed by dipping the p-Si in 3:1 sulfuric acid - hydrogen peroxide mixture for 1.0 min. They are further cleaned with diluted HCL and then double distilled water. MoS_2 Nano films are coated on the p-Si, placed at different temperatures of 400, 450, 500 and 550°C. The contacts are extended on both sides of the prepared MoS_2/p-Si diode using silver paste blended with isoamyl acetate. The schematic diagram of fabricated p-Si/n-MoS_2 diode is shown in Fig. 2

2.4 Characterization

The structural analyses of the samples were carried out using a Rigaku Ultima III XRD with Cu Kα radiation of continuous scanning with PSD mode. RAMAN Spectra was analyzed by confocal raman spectra(WiTec Alpha 300, Germany). The morphological studies were done using a RA-ZEI-001 model FESEM (Code R14401, CARL ZEISS) equipped with EDAX setup (QUANTAX 200, CODE 1103-0000:400, BRUKER). A JASCO UV-Vis spectroscope was used to study optical properties of the prepared samples, in the range 200 - 900 nm. A Keithley 6517-B electrometer and a PEC-L01S solar simulator were used to carry out the electrical properties of the MoS_2 diodes.

3 Results and discussion

3.1 XRD analysis

Fig. 3 displays XRD patterns of MoS_2 thin films grown at 400, 450, 500 and 550^oC respectively. The peaks for all the films prepared at different temperatures are found matching well with the JCPDS No 037-1492 which conforming hexagonal crystal structure of MoS_2 films with. From XRD pattern, it is very evident that the grown films are preferentially oriented towards (002) at 400-550^oC. The XRD also displays emergence or growth of new peaks with temperature. For example, the (103) peak for the film grown at 400^oC and (021) peak for the film grown at 450^{o}C are emerged with considerably high intensity compared to the films grown at 400^{o}C. However, the film gown at 550^{o}C doesn't show any particular preferential orientation and the intensity of (021) peak has reached above (002) peak. The (021) peak is related to MoO_3 which are found to be started to grown after 400 ^{o}C indicating the secondary phase (Orthorhombic) due to the oxidization during deposition at higher temperature. This result clearly indicates that the substrate temperature is strongly influences the MoS_2 thin films.The (021) peak matched with JCPDS file No. 05-508 [39]. However, all other peaks are related to MoS_2 films (Hexagonal). It was also noted that the FWHM (β) for the peaks are increasing with the growth temperature and could be attributed to the increasing crystallite sizes with the temperature. Scherer formula was employed to estimate the crystallite sizes of the thin films, and the growing crystallite sizes (D) with the deposition temperature were confirmed. Also, microstrain (ε) values, dislocation density (δ) and stacking fault probability (SF) values were estimated using the relations,

$$\varepsilon = \beta \cot(\theta)/4 \quad (1)$$

$$\delta = 1/D^2 \quad (2)$$

$$SF = [2\pi^2/(45\sqrt{3}\tan(\theta))]\Delta(2\theta) \quad (3)$$

where $\Delta(2\theta)$ is the observed shift in the 2θ positions. The obtained results are tabulated in **Table 1.** The ε, δ and SF values are found decreasing with the deposition temperature. Similar observations have been observed for the CdSe thin films prepared by thermal evaporation. The decreasing tendency of number of dislocations per unit area and stacking fault could be due to the increasing crystallite sizes with temperature and rearrangements happening with the increasing temperature. The stacking fault was calculated based on all the peaks observed from XRD. The stacking fault is referred to the deviation in the stacking sequence of the hexagonal wurtzite structure. So, the decrease in SF could mean a better stacking sequence in the structure.

3.2 Raman analysis

The Raman spectra for MoS_2 thin films prepared at different temperature as 400˚C, 450, 500, 550 ^{o}C are shown in figure 4 (a-d). A small shoulder peak observed at 286 cm^{-1} are corresponding to the E_{1g} mode of vibration due to the S-Mo-S layer of atoms where the intensity of this particular peak increased when increasing the annealing temperature **[40].** In figure 4 (a-d) two distinct peaks present in 384, 406 cm^{-1} which clearly confirms the MoS_2

phase in the sample. The intense less turn out at 384 cm^{-1} is attributed to E^1_{2g} phonon mode because of in-plane of vibration mode where the mode is terrace terminated vibration of opposite direction on sulfur atom and molybdenum atom **[41-42].** A characteristic peak at 406 cm^{-1} is corresponding to A_{1g} out-plane vibrational mode of sulfur atom in the direction perpendicular to the plane **[43].** Comparing the intensity difference between the two major activation modes of peaks the vertical plane of A_{1g} is much intense the E^1_{2g} that may be attributes to the polarization dependence of edge-terminated structure of MoS_2 **[44-46]**. The frequency difference between these two peaks was ~22 cm^{-1} which may be due to the monolayer behaviour of the MoS_2 **[47].** A broad shoulder peak observed at 454 cm^{-1} is represents the longitudinal acoustic mode of vibration **[48].** The sharp peak appeared in 820 cm^{-1} corresponding the mode of $2A_{1g}$ mode of vibration which is a second order mode peak due to the thermal effect on the sample this peak related to MoO_3 **[49].** Interestingly we can note that some additional weakly contributed peaks in the frequency range of 80 to 250 cm^{-1} appeared for the film prepared at 500°C which may be the structural change due to the change of temperature.

3.3 FESEM and EDX

Surface morphologies of the MoS_2 thin films prepared at 400, 450, 500 and 550°C deposition temperatures are depicted in FESEM images, in **Fig. 5(a-d).** From **Fig. 5**, the grains are formed as the elongated irregular rod structures. However, with the temperatures, the grain sizes are increasing and becoming more closely packed. The films grown at 550°C show an apparent unidirectional growth of majority of the grains. The micrographs also show dense layered structure of MoS_2 films, and thus might be exhibiting an indirect bandgap nature. the EDAX spectrum of the MoS_2 thin films with different deposition temperatures is shown in **Fig. 6.** From EDX spectrum, the important elements like Mo, S and O have been confirmed on the coated MoS_2 films. The obtained atomic ratio (%) of Mo is 13.48, 16.59, 12.18 and 9.54 for 400, 450, 500, 550 °C. Similarly, atomic ratio (%) of O and S are 61.56, 37.43, 58.46, 62.76 and 11. 23, 10.09, 2.58, 1.50 for 400, 450, 500, 550 °C. Other impurities like C, Na, Ca, Si was also observed due to the glass substrates. At higher substrate temperature, the atomic ratio (%) of Mo and S decreased and the O % increased. The substrate temperature strongly influences the composition of the MoS_2 films.

3.4 UV-Vis

Fig. 7 a & b represents optical absorption and transmission spectra of MoS_2 films prepared at various deposition temperatures. The absorption spectra show strong absorption region below 350 nm. The transmission spectra also validate this observation. The maximum transmission of ~50% is observed for the pure MoS_2 film, which was found systematically decline with the deposition temperature. The reason for this lowering of transmission could be attributed to the increasing crystallite size with the increasing deposition temperature. Also, red shifts in the absorption edges can be seen from these spectra with the increasing growth temperature, and could be attributed to the increasing crystallite sizes. The absorption coefficients, α were calculated from the transmittance (T) using the following relation,

$$\alpha = \frac{2.203\ x \log\left(\frac{1}{T}\right)}{t} \quad (4)$$

Where T is the transmittance and t is the thickness of the MoS_2 films.

The band gap relation of the MoS_2 films can be obtained using the relationship

$$(\alpha h\nu)^2 = A(h\nu - E_g) \quad (5)$$

Where $h\nu$ is the incidence photon energy, E_g is the band gap energy and A is a constant. The value of E_g were estimated from the linear extrapolations of $(\alpha h\nu)^2$ vs. $h\nu$ plots, on $h\nu$ axis. From the plots, it was very much evident that the band gap values were systematically decreasing with the deposition temperature. The bulk MoS_2 is an indirect bandgap (E_g=1.29 eV) semiconductor with multilayers, whereas monolayer MoS_2 is a direct bandgap material, with E_g=1.9 eV [50-53]. From the **Fig. 7c,** the direct band estimations are almost in the same range, and are higher than the reported value for bulk samples. The reason could be attributed to the highly nanostructured growth of the prepared MoS_2 samples [53]. The observed red shift or the reducing tendency of the band gap with the growth temperature is due the increasing crystallite size with the temperature. The thicknesses of the films were estimated to be around 400 nm, and it could be inferred that the band gap energies of prepared films are of indirect in nature. Moreover, the variations of optical parameters with temperature are presented in **Fig. 7d**. Both absorption and extinction coefficient are increased linearly with temperature.

3.5 Electrical conductivity

The electrical behaviour of the spray coated MoS_2 thin films were studied through a facile two-point probe setup. The change of current values with temperature were recorded by applying a positive voltage ranging from 0 to 100 (step of 20) as shown in **Fig. 8a**. It is noted from the **Fig. 8a** that the current values are strongly dependant with temperature. The higher temperature showed a huge difference in current values when compared to lower temperature. The formation of oxygen vacancy can influence the electrical characteristics of the samples. The resistivity of the films was determined from the I-V characteristics by the following equation.

$$\rho = R\left(\frac{A}{t}\right)\Omega cm \quad (6)$$

Numerous literatures advocate that the electrical resistivity of the thin film depends on the crystallizations of the prepared film, type of surface structure, deposition technique and preparative parameters, etc. The resistivity of the present MoS_2 films is favorably reduced as 7.29×10^7, 4.33×10^7, 7.77×10^6, 5.99×10^6 **Ω** cm for 400, 450, 500, 500 ºC. Decrease in resistivity with increasing temperature is accredited to the creation of more oxygen vacancy during the film deposition and increase in crystallite size of the MoS_2 films [54]. The conductivity of the samples was assessed by the relation and listed in Table 2.

$$\sigma_{dc} = \frac{t}{RA} \quad (7)$$

The Arrhenius plot **(Fig.8b)** showed that the large variation in the electrical conductivity with inverse temperature and also specifies the existence of double conduction mechanisms (CM). For high-temperature part is related to the grain boundary scattering limited CM and low-temperature part is related to variable range hopping CM [55]. The substrate temperatures effectively improve the electrical conductivity particularly 550 ºC as shown in **Fig.8c.** The calculated average conductivity values were found to be increased from 1.730×10^{-8} to 3.877×10^{-7} S/cm with substrate temperature. The obtained conductivity values are suggesting the semiconducting nature of the MOS_2 films. The conductivity maximum of 3.877×10^{-7} S/cm was observed at higher crystallite size of MoS_2 film. We observed that the MoS_2 film with higher crystallite size can facilitate to enhance the conductivity of the films. The decrease in the grain-boundary scattering also aids to enhances the film conductivity [56]. The activation energy (E_a) of the MoS_2 films was determained from the slop of Arrhenius plot. The E_a was found to decreased from 0.129 to 0.038 eV with substrate temperature. The variation in E_a is mostly due to the expansion in crystallinity, thickness of the film and lesser defect concentration.

3.6 I-V characteristics of p-Si/n-MoS_2 junction diodes

The forward and reverse characteristics of the fabricated p-Si/n-MoS_2 junction diode are shown in **Fig. 9a.** To understand the photo-response of the present diode, we have measured both dark and photocurrent of the diode by applying bias voltage -4 to +4 V. For photocurrent measurement, the intensity of the light was fixed as 100 mW/cm^2. The wavelength range of the solar simulator is ~ 400-1100 nm (as per JIS C 8912 standard). The irradiance comes through an air mass 1.5 G filter and fall on the diode. The thickness of the emitter layer is around 500-600 nm. From the p-Si/n-MoS_2 diode curve, it is clear that all the diode showed positive photo-response at 100 mW/cm^2 relatively under dark condition. Moreover, the obtained superior forward current and weaker reverse current implying the photo-conducting properties of the fabricated diode. The current transport mechanism of p-Si/n-MoS_2 is studied and described by traditional thermionic emission (TE) principle as follows [57-59].

$$\mathrm{I} = \mathrm{I}_0 \left[\exp\left(\frac{\mathrm{qV}}{\mathrm{nK_BT}} - 1\right)\right] \quad (8)$$

where I_o, q, V, n, k_B and T are the reverse saturation current, charge of electron, applied potential, ideality factor, Boltzmann constant and temperature. The ideality factor (n) and barrier height (Φ_B) are the key parameters to understand the device performance. The n and Φ_B of the p-Si/n-MoS_2 diodes were determined from semi-logarithmic plot **(Fig. 9b)** through the following equations [57,58].

$$\mathrm{n} = \frac{\mathrm{q}}{\mathrm{k_BT}}\left(\frac{\mathrm{d}}{\mathrm{d(ln(J))}}(\mathrm{V})\right) \quad (9)$$

$$\Phi_\mathrm{B} = \frac{\mathrm{k_BT}}{\mathrm{q}}\ln\left(\frac{\mathrm{A}^*A\mathrm{T}^2}{\mathrm{J}_0}\right) \quad (10)$$

Here, A* = 32 A/cm^2 K^{-2}, the effective Richardson constant for p-Si.

The estimated n and $\Phi_B$values were compared in Table 3. The estimated n and Φ_B values are very sensitive with substrate temperature, especially at higher. The p-Si/n-MoS_2 diodes showed a favourable trending of increasing ideality factor with reducing barrier height while decreasing substrate temperature from 550 to 400 ºC. Many literatures have been reported a similar behaviour in various junction diodes [57-63]. At lower temperature, the electron doesn’t have enough energy to pass the barrier potential. But, at higher temperature, electron gains adequate energy to cross this barrier. Hence, our diode revealed better diode performance at higher temperature. Besides, all the diodes recorded higher photocurrent under light exposed condition i.e 100 mW/cm^2 which is attributed to due to the formation of superior photo-carrier charge cupules with lessor recombination. Remarkably, the p-Si/n-

MoS_2 diode fabricated at 550 ºC revealed minimum n values of 2.23. The 400 and 450 ºC showed higher n values due to the weak temperature, lesser separation of charge cupules, image force lowering, tunnelling. Also, the native oxide layer SiO_2 will be formed during deposition which may also affect the ideality factor of the diode. Moreover, the Φ_B values varied from 0.541 to 0.729 eV with temperature. The excremental Φ_B is mostly influenced by the diffusion of minority charge carriers between n-side and p-side and thickness of the depletion region.

4. Conclusion

A nanostructured MoS_2 thin films and p-Si/n-MoS_2 diodes were successfully grown at different substrate temperatures using JNSP method. The impacts of growth temperature on various features including structural and electrical characteristics of MoS_2 thin films were studied. The XRD patterns confirm the hexagonal and Orthorhombic phase of the MoS_2/ MoO_3 thin films temperature between 400 to 550 °C. The average crystallite size of MoS_2 thin film changed from 31.16 to 45.50 nm. From FESEM results, the films grown at 550^{o}C show an apparent unidirectional growth of majority of the grains. The maximum absorption and the band gap minimum (of 2.6 eV) were observed for the film deposited at 550°C. From I-V characteristics, the resistivity of MoS_2 was favorably reduced while increasing substrate temperature. The n-MoS_2/p-Si junction diode recorded lower n value under light conations, exhibiting the photo detection nature of the diode. This photo response behavior makes these diodes suitable for photo detector applications.

References

[1] A. Sharma Akhil Sharma, Reyhaneh Mahlouji , Longfei Wu, Marcel A. Verheijen, Vincent Vandalon, Shashank Balasubramanyam, Jan P. Hofmann, W. M. M. (Erwin) Kessels, Ageeth. A. Bol1, Large area, patterned growth of 2D MoS2 and lateral MoS2-WS2 heterostructures for nano-and opto-electronic applications, Nanotechnology 31 (2020) 1-25.

[2] Xudong Wang, Chunsen Liu, Yan Chen, Guangjian Wu, Xiao Yan, Hai Huang, Peng Wang, Bobo Tian,Zhenchen Hong, Yutao Wang, Shuo Sun, Hong Shen, Tie Lin,

Weida Hu, Minghua Tang, Peng Zhou,Jianlu Wang, Jinglan Sun, Xiangjian Meng, Junhao Chu and Zheng Li, Ferroelectric FET for nonvolatile memory application with two-dimensional MoSe2 channels, *2D Mater* 4 (2017) 025036.

[3] Nurul Ain Abd Malek, Nabilah Alias, Akrajas Ali Umar, Xin Zhang, Xiaoguo Li, Siti Khatijah Md Saad, Nur Adliha Abdullah, Haijuan Zhang, Zhenhua Weng, Zejiao Shi, Chongyuan Li, Mohd Mustaqim Rosli, and Yiqiang Zhan, Enhanced Charge Transfer in Atom-Thick 2H–WS2 Nanosheets Electron Transport Layers of Perovskite Solar Cells, Sol. RRL 2020, 4, 2000260 (1 of 11)

[4] F. Urban, N. Martucciello, L. Peters, N. McEvoy, and A. Di Bartolomeo, Environmental effects on the electrical characteristics of back-gated WSe 2 field-effect transistors, Nanomaterials 8 (2018) 901.

[5] Lu Li , Ruidong Lv , JiangWang , Zhendong Chen , Huizhong Wang , Sicong ,Liu,Wei Ren , Wenjun Liu , and Yonggang Wang , Optical nonlinearity of ZrS_2 and applications in fiber laser, Nanomaterials 9 (2019) 315.

[6] Y. Xiong, H. W. Chen, D. W. Zhang, and P. Zhou, Electronic and Optoelectronic Applications Based on ReS2, Phys. Status Solidi - Rapid Research Letter 13 (2019) 1800658 1–14.

[7] M. Ye, D. Winslow, D. Zhang, R. Pandey, and Y. K. Yap, Recent advancement on the optical properties of two-dimensional molybdenum disulfide (MoS2) thin films, Photonics 2 (2015) 288–307.

[8] Sina Najmaei, Xiaolong Zou, Dequan Er, Junwen Li, Zehua Jin, Weilu Gao, Qi Zhang, Sooyoun Park, Liehui Ge, Sidong Lei, Junichiro Kono, Vivek B Shenoy, Boris I. Yakobson, Antony George, Pulickel M Ajayan, and Jun Lou, "Tailoring the physical properties of molybdenum disulfide monolayers by control of interfacial chemistry," Nano Letters 14 (2014) 1354–1361.

[9] Juan Du1, Qingkai Wang1, Guobao Jiang1, Changwen Xu, Chujun Zhao, Yuanjiang Xiang, Yu Chen,Shuangchun Wen & Han Zhang, Ytterbium-doped fiber laser passively mode locked by few-layer Molybdenum Disulfide (MoS_2) saturable absorber functioned with evanescent field interaction, Scitific Reports 4 (2014) 6346 1–7.

[10] J. Park, N. Choudhary, J. Smith, G. Lee, M. Kim, and W. Choi, Thickness modulated MoS_2 grown by chemical vapor deposition for transparent and flexible electronic devices, Applied Physics Letters 106 (2015) 012104.

[11] Jiu Li, Qingqing Ji, Saisai Chu, Yanfeng Zhang, Yan Li, Qihuang Gong, Kaihui Liu & Kebin Shi, Tuning the photo-response in monolayer MoS_2 by plasmonic nano-antenna, Scitific Reports 6 (2016) 23626.

[12] S. K. Pradhan, B. Xiao, and A. K. Pradhan, Enhanced photo-response in p-Si/MoS_2 heterojunction-based solar cells, Solar Energy Material Solar Cells 144 (2016) 117–127.

[13] Rui Cheng, Dehui Li, Hailong Zhou, Chen Wang, Anxiang Yin,Shan Jiang, Yuan Liu, Yu Chen,Yu Huang, and Xiangfeng Duan, Electroluminescence and photocurrent generation from atomically sharp WSe_2/MoS_2 heterojunction p-n diodes, Nano Letters, 10 (2014) 5590–5597.

[14] Yexin Deng, Zhe Luo, Nathan J. Conrad, Han Liu, Yongji Gong, Sina Najmaei, Pulickel M. Ajayan,Jun Lou, Xianfan Xu, and Peide D. Ye, Black phosphorus-monolayer MoS_2 van der Waals heterojunction p-n diode, ACS Nano 8 (2014) 8292–8299.

[15] Deep Jariwala, Vinod K. Sangwan, Chung-Chiang Wu, Pradyumna L. Prabhumirashi, Michael L. Geier, Tobin J. Marks, Lincoln J. Lauhon, and Mark C. Hersam., Gate-tunable carbon nanotube-MoS2 heterojunction p-n diode, Proceedings of the National Academy Science 110 (2013) 45 18076–18080.

[16] H. Wang, C. Li, P. Fang, Z. Zhang, and J. Z. Zhang, Synthesis, properties, and optoelectronic applications of two-dimensional MoS_2 and MoS_2-based heterostructures, Chemical Society Revews 47 (2018) 6101–6127.

[17] J. Jian, H. Chang, and T. Xu, Structure and properties of single-layer MoS_2 for nano-photoelectric devices, Materials (Basel) 12 (2019) 1–10.

[18] Yexin Deng, Zhe Luo, Nathan J. Conrad, Han Liu, Yongji Gong, Sina Najmaei, Pulickel M. Ajayan, Jun Lou, Xianfan Xu, and Peide D. Ye, Ehancement of

photovoltaic response in multilayer MoS_2 induced by plasma doping," ACS Nano 8 (2014) 5270–5281.

[19] Yuka Tsuboi,a Feijiu Wang,a Daichi Kozawa,a Kazuma Funahashi,b Shinichiro Mouri, aYuhei Miyauchi, a Taishi Takenobub and Kazunari Matsuda, Enhanced photovoltaic performances of graphene/Si solar cells by insertion of a MoS_2 thin film, Nanoscale 7 (2015) 14476–14482.

[20] Meng-Lin Tsai, Sheng-Han Su, Jan-Kai Chang, Dung-Sheng Tsai,Chang-Hsiao Chen, Chih-I Wu,Lain-Jong Li, Lih-Juann Chen, and Jr-Hau He Monolayer MoS_2 heterojunction solar cells, American Chemical Society 8 (2014) 8317–8322.

[21] Chung-Che Huang,a Feras Al-Saab,a Yudong Wang,b Jun-Yu Ou,a John C. Walker,c Shuncai Wang,c Behrad Gholipour,a Robert E. Simpsond and Daniel W. Hewak, Scalable high-mobility MoS_2 thin films fabricated by an atmospheric pressure chemical vapor deposition process at ambient temperature, Royal Society of Chemistry 6 (2014) 12792–12797.

[22] C. Jiang, S. L. Rumyantsev, R. Samnakay, M. S. Shur, and A. A. Balandin, High-temperature performance of MoS_2 thin-film transistors: Direct current and pulse current-voltage characteristics, Journal of Applied Physics 117 (2015) 6.

[23] Y. Zhang, J. Ye, Y. Matsuhashi, and Y. Iwasa, Ambipolar MoS_2 Thin Falke Transi.Pdf, Nano Letter 12 (2012) 1136–1140.

[24] Z. Wang and B. Mi, Environmental Applications of 2D Molybdenum Disulfide (MoS_2) Nanosheets, Environmental Science and Technology 51 (2017) 8229–8244.

[25] S. H. Baek, Y. Choi, and W. Choi, Large-Area Growth of Uniform Single-Layer MoS_2 Thin Films by Chemical Vapor Deposition, Nanoscale Research Letter. 10 (2015) 4–9.

[26] Lin Wang, Li Chen, Swee Liang Wong, Xin Huang, Wugang Liao, Chunxiang Zhu,Yee-Fun Lim, Dabing Li, Xinke Liu,Dongzhi Chi,and Kah-Wee Ang, Electronic Devices and Circuits Based on Wafer-Scale Polycrystalline Monolayer MoS_2 by Chemical Vapor Deposition, Advanced Electronic. Matererials. 5 (2019) 1–10.

[27] J. Pu, L. J. Li, and T. Takenobu, Flexible and stretchable thin-film transistors based on molybdenum disulphide, Physics Chemistry Chemical Physic 16 (2014) 14996–15006.

[28] Panpan Zhang, Sheng Yang, Roberto Pineda-Gómez, Bergoi Ibarlucea, Ji Ma, Martin R. Lohe,Teuku Fawzul Akbar, Larysa Baraban, Gianaurelio Cuniberti, and Xinliang Feng, Electrochemically Exfoliated High-Quality 2H-MoS2 for Multiflake Thin Film Flexible Biosensors, Nano micro Small 15 (2019) 1901265 1–10.

[29] Zongyou Yin, Xiao Zhang, Yongqing Cai, Junze Chen, Jen It Wong, Yee-Yan Tay, Jianwei Chai,Jumiati Wu, Zhiyuan Zeng, Bing Zheng, Hui Ying Yang, and Hua Zhang, "Preparation of MoS_2-MoO_3 hybrid nanomaterials for light-emitting diodes," Angewante Chemie 53 (2014) 12560–12565.

[30] Namjo Jeong, Han-ki Kim, Won-sik Kim, Ji Yeon Choi, Kyo-sik Hwang, Joo-youn Nam, Ji-hyung Han, Eun-Jin Jwa, Yoon-Cheul Jeong, Direct synthesis, characterization, and reverse electrodialysis applications of MoS_2 thin film on aluminum foil, Materials Characterization 164 (2020) 110361.

[31] Dahai Lia, Xiongfei Songb, Jiping Xua, Ziyi Wanga, Rongjun Zhanga, Peng Zhoub,Hao Zhanga, Renzhong Huangc, Songyou Wanga, Yuxiang Zhenga, David Wei Zhangb,Liangyao Chena , Optical properties of thickness-controlled MoS_2 thin films studied by spectroscopic ellipsometry, Applied Surface Science 421 (2017) 884–890.

[32] S. K. Srivastava and B. N. Avasthi, Preparation and characterization of molybdenum disulphide catalysts, Journal of Material Science 28 (1993) 5032–5035.

[33] K. M. Garadkar, A. A. Patil, P. P. Hankare, P. A. Chate, D. J. Sathe, and S. D. Delekar, MoS_2: Preparation and their characterization, Joural of Alloys Compound 487 (2009) 786–789.

[34] B. Pietrzyk, S. Miszczak, Ł. Kaczmarek, and M. Klich, Low friction nanocomposite aluminum oxide/MoS_2 coatings prepared by sol-gel method, Ceram. International 44 (2018) 8534–8539.

[35] Nurul Ain Abd Malek , Nabilah Alias , Siti Khatijah Md Saad , Nur Adliha Abdullah , Xin Zhang , Xiaoguo Li , Zejiao Shi , Mohd Mustaqim Rosli , Tengku Hasnan Tengku Abd Aziz, Akrajas Ali Umar , Yiqiang Zhan , Ultra-thin MoS2 nanosheet for electron transport layer of perovskite solar cells, Optical Materials 104 (2020) 109933.

[36] B. Chamlagain and S. I. Khondaker, Electrical properties tunability of large area MoS_2 thin films by oxygen plasma treatment , Applied Physics Letter 116 (2020) 223102.

[37] J. H. Kim, J. K. Kim, and Y. C. Kang, Sodium-ion storage performances of MoS_2 nanocrystals coated with N-doped carbon synthesized by flame spray pyrolysis, Applied Surface Science, 523 (2020) 146470.

[38] P. Venkateswari, P. Thirunavukkarasu, M. Ramamurthy, M. Balaji, J.Chandrasekaran, Optimization and characterization of CuO thin films for P-N junction diode application by JNSP technique, Optik - International Journal for Light and Electron Optics S0030-4026 (2017) 30434-5.

[39] Akhilesh Pandey, Anoushka Dhaka, Chandni Kumari, Janesh Kaushik, Aman Arora, Shankar Dutta, Ambesh Dixit$, and R. Raman, RF Sputtered MoO_3 Thin Film on Si (100) for Gas Sensing Applications, Defence Science Journal, 70 (2020) 505-510

[40] J.M.Chen, C.S.Wang ,second order raman spectrum of MoS_2., solid state communication,14 (1974) 854.

[41] D. Kong, H.Wang,J.J. Cha, M.Pasta, K.J. Koski, J.Yao, Y.Cui, Synthesis of MoS_2 and MoSe2 Films with Vertically Aligned Layers Nano Lett. 13 (2013) 1341.

[42] W.Wang, X.Chen,X.Zeng , S.Wu, Y.Zeng,Y.Hu, S. Xu, G. Zhou, H.Cui, Investigation of the Growth Process of Continuous Monolayer MoS_2 Films Prepared by Chemical Vapor Deposition, Journal of Electronic Materials, 47 (2019) 5509.

[43] Growth of wafer-scale MoS_2 monolayer by magnetron sputtering, J. Tao,J.Chai,X.Lu, L.M.Wong,T.I.Wong,J.Pan, Q. Xiong, D.Chia,S.Wang, Nanoscale, 7 (2015) 2497.

[44] M.R Gao, M.K.Y.Chan, Y. Sun, Edge-terminated molybdenum disulphide with a 9.4-Å

interlayer spacing for electrochemical hydrogen production. National. Communication. 6 (2015) 7493.

[45] Y.Sun, K. Liu, X.Hong, M.Chen, J.Kim, S.Shi, J.Wu, A.Zettl, F.Wang, Probing Local Strain at MX(2)–Metal Boundaries with Surface Plasmon-Enhanced Raman Scattering. Nanoscience Letter. 14 (2014) 5329.

[46] B.Élodie,A.Pavel, B.Gilles, U.Denis, L.Stéphane, Resonance Raman spectroscopy as a probe of the crystallite size of MoS_2 nanoparticles, Comptes Rendus Chimie , 19 (2016) 1310.

[47] Y.T. Ho, C.H.Ma, T.T.Luong, L.L.Wei, T.C.Yen, W.T.Hsu, W.H.Chang, Y.C.Chu, Y.Y.Tu, K. P. Pande, E.Y.Chang, Layered MoS2 grown on c -sapphire by pulsed laser deposition , 9 (2015) 187

[48] Y.Yixin , A.Kelong , L.Pengfei, W.Qufu, MoS_2 Coexisting in 1T and 2H Phases Synthesized by Common Hydrothermal Method for Hydrogen Evolution Reaction, Nanomaterials 9 (2019) 844.

[49] Growth and characterization of molybdenum oxide nanorods by RF magnetron sputtering and subsequent annealing, Navas, R Vinodkumar, K J Lethy, A P Detty, V Ganesan, V Sathe and V P Mahadevan Pillai, J. Phys. D: Appl. Phys. 42 (2009) 175305

M. Placidi, M.Dimitrievska, V.I.Roca, X.Fontané, A.C.Gomez, A.P.Tomás, N. Mestres, M. E.Rodriguez, S.L.Marino, M. Neuschitzer, Multiwavelength excitation Raman thin scattering analysis of bulk and two dimensional MoS2: Vibrational properties of atomically MoS2 layers, 2D Mater , 2 (2015) 35006.

[50] J. Ryou, Y.-S. Kim, S. Kc, K. Cho, Monolayer MoS_2 Bandgap Modulation by Dielectric Environments and Tunable Bandgap Transistors, Scientific Reports, 6 (2016) 29184.

[51] I. Sta, M. Jlassi, M. Kandyla, M. Hajji, P. Koralli, R. Allagui, M. Kompitsas, H.

Ezzaouia, Hydrogen sensing by sol–gel grown NiO and NiO: Li thin films, Journal of Alloys and Compounds 626 (2015) 87-92.

[52] K.F. Mak, C. Lee, J. Hone, J. Shan, T.F. Heinz, Atomically Thin MoS_2: A New Direct-Gap Semiconductor, Physics Review Letter 105 (2010) 136805.

[53] M.M. Aslam, S.M. Ali, A. Fatehmulla, W.A. Farooq, M. Atif, A.M. Al-Dhafiri, M.A. Shar, Growth and characterization of layer by layer CdS-ZnS QDs on dandelion like TiO_2 microspheres for QDSSC application, Materials Science in Semiconductor Processing, 36 (2015) 57-64.

[54] E. M. Mkawi, K. Ibrahim, M. K. M. Ali, M. A. Farrukh, A. S. Mohamed, The effect of dopant concentration on properties of transparent conducting Al-doped ZnO thin films for efficient Cu2ZnSnS4 thin-film solar cells prepared by electro deposition method, Applied Nanoscience 5 (2015) 99 3–1001

[55] K.M. Garadkar, A.A. Patil, P.P. Hankare, P.A. Chate, D.J. Sathe, S.D. Delekar, MoS_2: Preparation and their characterization, Journal of Alloys and Compounds 487 (2009) 786–789

[56] R. Siva Prakash, C. Mahendran, J. Chandrasekaran, R. Marnadu, S. Maruthamuthu, Impact of Substrate Temperature on the Properties of Rare-Earth Cerium Oxide Thin Films and Electrical Performance of p-Si/n-CeO_2 Junction Diode, Journal of Inorganic and Organometallic Polymers and Materials (2020) https://doi.org/10.1007/s10904-020-01667-7

[57] A Buyukbas-Ulusan, S Altındal-Yerişkin, A Tataroğlu, Forward and reverse bias current–voltage (I–V) characteristics in the metal–ferroelectric–semiconductor (Au/$SrTiO_3$/n-Si) structures at room temperature, Journal of Materials Science: Materials in Electronics 29 (2018) 16740-16746.

[58] AB Uluşan, A Tataroğlu, Y Azizian-Kalandaragh, Ş Altındal, On the conduction mechanisms of Au/(Cu2O–CuO–PVA)/n-Si (MPS) Schottky barrier diodes (SBDs) using current–voltage–temperature (I–V–T) characteristics, Journal of Materials Science: Materials in Electronics 29 (2018) 159-170.

[59] A Tataroğlu, Ş Altındal, The analysis of the series resistance and interface states of MIS Schottky diodes at high temperatures using I–V characteristics, Journal of Alloys

and Compounds 484 (2009) 405-409.

[60] R. Marnadu, J. Chandrasekaran, P. Vivek, V. Balasubramani, S. Maruthamuthu, Impact of phase transformation in WO_3 thin films at higher temperature and its compelling interfacial role in $Cu/WO_3/p\text{-}Si$ structure schottky barrier diodes, Zeitschrift Für Physikalische Chemie, 234, (2020) 355-379.

[61] R. Marnadu, J. Chandrasekaran, S. Maruthamuthu, V. Balasubramani, P. Vivek, R. Suresh, Ultra-high photoresponse with superiorly sensitive metal-insulator-semiconductor (MIS) structured diodes for UV photodetector application. Applied Surface Science, 480 (2019) 308–322.

[62] P. Sumathi, J. Chandrasekaran, R. Marnadu, S. Muthukrishnan, S. Maruthamuthu, Synthesis and characterization of tungsten disulfide thin films by spray pyrolysis technique for $n\text{-}WS_2/p\text{-}Si$ junction diode application, Journal of Materials Science: Materials in Electronics, 29 (2018) 16815–16823.

[63] P. Vivek, J. Chandrasekaran, R. Marnadu, S. Maruthamuthu, V. Balasubramani, P. Balraju, Zirconia modified nanostructured MoO_3 thin films deposited by spray pyrolysis technique for $Cu/MoO_3\text{-}ZrO_2/p\text{-}Si$ structured Schottky barrier diode application, Optik, 199 (2019) 163351.

Fig. 1. Schematic diagram of jet nebulizer spray pyrolysis setup

Fig. 2. Schematic diagram of p-Si/n-MoS2 junction diode

Fig. 3. XRD patterns of MoS_2 thin films prepared at 400, 450, 500 and 550 ^{o}C with JCPDS.

Fig. 4. Raman spectra for MoS_2 thin film coated at different temperature.

Fig. 5. SEM images of the MoS_2 thin films prepared at different deposition temperatures

Fig. 6. EDX spectrum of the MoS_2 thin films

Fig. 7. a) Optical absorption, b) transmission and c) Tauc's plot for indirect and d) variations of optical parameters of MoS_2 thin films prepared at different deposition temperatures

Fig. 8. (a) I-V characteristics of MoS_2 films for different substrate temperature (b) Arrhenius plot (c) Variation of activation energy and conductivity with substrate temperature

Fig. 9. (a) I-V characteristics (b) semi-logarithmic plot of p-Si/n-MoS_2 diode for different substrate temperature

Table 1. Structural parameter of MoS_2 thin films for various temperature

Substrate Temperature (°C)	**Crystalline Size D (nm)**	**Micro strain (ε)**	**Dislocation density (δ) ×10^{-14} (lines cm^{-2})**	**Stacking fault (SF) × 10^{-2}**
400	31.16	0.0176	4.605	0.5402
450	35.68	0.0139	2.564	0.4481
500	37.37	0.0126	2.071	0.3215
550	45.02	0.0090	1.915	0.2546

Table 2. Electrical parameters of MoS_2 films for different substrate temperature

Substrate temperature (°C)	Average Resistivity (ρ) (Ω cm)	Average conductivity (S/cm)	Average activation energy (E_a) (eV)
400	7.29×10^7	1.730×10^{-8}	0.129
450	4.33×10^7	3.578×10^{-8}	0.083
500	7.77×10^6	1.228×10^{-7}	0.064
550	5.99×10^6	3.877×10^{-7}	0.038

Table 3. p-Si/n-MoS_2 diode parameters for different substrate temperature

Substrate temperature (°C)	Barrier height (Φ)		Ideality factor (n)	
	Dark	Light	Dark	Light
400	0.55	0.54	5.80	4.40
450	0.60	0.62	4.57	3.32
500	0.62	0.66	4.51	2.69
550	0.68	0.72	3.23	2.23